3D porous alumina/graphene hybrids prepared by atomic layer deposition and their performance for water treatment

Rabita Mohd Firdaus, Claudia de Melo, Sylvie Migot, Mélanie Emo, Jean-François Pierson, Abdul Rahman Mohamed, Brigitte Vigolo

3D porous alumina/graphene hybrids prepared by atomic layer deposition and their performance for water treatment

Rabita Mohd Firdaus[a,b], *Claudia De Melo*[a,¥], *Sylvie Migot*[a], *Mélanie Emo*[a], *Jean-François Pierson*[a], *Abdul Rahman Mohamed*[b,*], *Brigitte Vigolo*[a,*]

[a] Université de Lorraine, CNRS, IJL, F-54000 Nancy, France

[b] School of Chemical Engineering, Engineering Campus, Universiti Sains Malaysia, 14300 Nibong Tebal, Seberang Perai Selatan, P. Pinang, Malaysia

[¥]present address: Université d'Orléans, CNRS, ICMN, 1b rue de la Férollerie, Orléans Cedex 2, France

Corresponding authors

* Dr. Brigitte Vigolo; email: brigitte.vigolo@univ-lorraine.fr; Tel: +33 372742980; ORCID: 0000-0002-1463-0121

* Dr. Prof. Abdul Rahman Mohamed: chrahman@usm.my; ORCID: 0000-0002-5418-5456

KEYWORDS hybrid materials; alumina; graphene oxide and reduced graphene oxide; atomic layer deposition; dye removal; water treatment

ABSTRACT Metal / carbon hybrids have impressive potential of applications in many fields: catalysis, energy conversion and storage, environmental. However, further efforts are needed to achieve a better control of homogeneity of the metal oxide deposit on the carbon surface to provide reliable synthesis approaches of metal / carbon hybrids. In this work, atomic layer deposition is used to prepare 3D porous alumina / reduced graphene oxide hybrid monoliths. We show that atomic layer deposition, even though rarely reported to prepare metal oxide / carbon hybrids, allows a conformal coating onto the graphene nanosheet surface. In-depth advanced characterization have been performed thanks to a coupled approach consisting of the preparation of lamellas of the porous hybrid by means of focused ion beam and their analysis by transmission electron microscopy. A good accessibility of the alumina precursors to the internal surface of the prepared 3D porous carbon monoliths was evidenced. The alumina / graphene hybrid prepared with 50 cycles of ALD deposit has a surface as high as 284 m^2 g^{-1}. As a proof-of-concept for the interest of the designed hybrids, they are tested for the removal of Congo red, a standard organic dye pollutant. 87 and 98 % of Congo red removal were reached at the first and the second step of adsorption proving the good adsorption performance and reusability ability of the de designed hybrid adsorbents. We believe that such multi-porous 3D alumina / graphene macrostructures that offers a favorable accessibility to the adsorption sites open interesting potentialities for pollution remediation applications.

1. Introduction

Since more than ten years, hybrid nanomaterials have emerged as a new class of materials of great interest among scholars. The strong coupling or synergistic interactions between the two nanomaterials over a large surface is able to induce emerging or exacerbated properties [1–3].

Combining metal oxides with carbon nanomaterials offers, in particular, the opportunity to develop multifunctional materials with a wide range of potential applications. They can especially be used as catalysts or adsorbents which is one of the key pillars for energy and environmental transition [4–6]. The quality of the available water and ecological systems on Earth is gradually degraded. The International Food Policy Research Institute (IFPRI) and Veolia Environment S.A. have projected for 2050 the water quality over the world based on three indices (nitrogen, phosphorus and biochemical oxygen demand (BOD)) for major river basins [7]. Their results have shown that a lot of countries situated on all the continents will be strongly impacted by serious risks for human beings and ecological systems. For remediation and depollution processes, designing efficient adsorbents is hence urgently demanded.

Al_2O_3 is thermally stable, insoluble in water and it is an electrical insulator having high hardness, mechanical strength and interesting catalytical properties which explains its industrial use in many applications. Al_2O_3 has in particular shown efficient adsorption properties of organic pollutants like dyes [8,9]. Wetness impregnation based on sol-gel or solution precipitation is the standard approach for metal oxide deposition on a support to prepare these hybrid adsorbents. Such methods requires subsequent washing and a final thermal drying treatment. These multistep approaches are simple to carry out but they have shown several limitations such as presence of impurities and redistribution and reaggregation on the support surface [10]. Under these conditions, accessibility of the reactant/adsorbate to the surface and the matter transfer are reduced due to the nonhomogeneous covering of the support surface and likely pore clogging. Moreover, the involved mechanisms are difficult to study and understand and the outcome performances can be strongly impacted and uncertain. Proposing synthesis approaches to produce hybrid nanoadsorbents with a reproducible, controlled and reliable process is currently

the core of the research works in the field. Alternative gas phase method like atomic layer deposition (ALD) [11], although still little used, appears as a powerful technique to lead to conformal homogeneous deposits of metal oxides like Al_2O_3 in a controlled manner [12].

Among the nanomaterials studied in the two last decades, graphene possesses a unique combination of remarkable chemical and physical properties: high surface area, stability, electron mobility, thermal conductivity, and mechanical strength [13]. For the purpose of overcoming the possible toxic effects and to improve recyclability and regeneration of adsorbents, development of 3D graphene assemblies in macrostructures (GAMs), also called monoliths, sponges, foams, aerogels… has been proposed. GAMs have generated a great interest among scholars over the past decade because they have shown high performances for applications in energy and environmental applications [14–19]. These GAMs provide a porous interconnected network with a good chemical stability and high accessible surface to develop new 3D porous metal oxide/GAM hybrid adsorbents [20–23].

Defect-free pristine graphene surface has been reported to inhibit the growth of Al_2O_3 due to the lack of reactive sites on the surface [24,25]. Different multi-step complex strategies have been proposed to induce efficient anchoring of Al_2O_3 precursors on graphene such as surface pretreatment by reactive gas or metal/metal oxide seed-layers and deposition of a sub-layer of organic species or polymers [25,26]. However these additives cannot be removed after the ALD process and they remain as impurities within the outcome Al_2O_3 / graphene hybrids. Among the graphene derivatives, graphene oxide (GO) and reduced GO (rGO) naturally bear a lot of functional groups that can act as seeding sites for alumina nucleation by ALD [27–29].

In the present work, 3D porous alumina / GAM hybrids have been designed by using ALD to deposit Al_2O_3 on the inner surfaces of GAMs. Added to standard scanning electron microscopy

(SEM), X-ray energy dispersive spectroscopy (EDS), advanced methods such as transmission electron microscopy (TEM) and associated electron energy loss spectroscopy (EELS) have been used for an in-depth characterization of porous alumina / graphene hybrids. The alumina deposition mechanism by ALD has been investigated and the developed hybrids have been tested for Congo red removal.

2. Materials and Methods

2.1. Materials and Chemicals

The used chemicals such as, graphite powder (purity 99.9995 %), sulphuric acid (H_2SO_4, 95–97 %), sodium nitrate ($NaNO_3$), potassium permanganate ($KMnO_4$), hydrogen peroxide (H_2O_2, 30%), hydrochloric acid (HCl, 37 %), potassium hydroxide (KOH), ammonia (NH_3, 25 %), L-ascorbic acid (vitamin C) were purchased from Sigma-Aldrich and used in this experiment as received. Trimethylaluminum (TMA) (purity min. 98 %) was purchased from Strem Chemicals, Inc.

2.2. Preparation of GO

The Hummers' method was used to synthesize GO from graphite powder [30]. The typical procedure is as follows: graphite (2 g) and $NaNO_3$ (2 g) were mixed with H_2SO_4 (50 mL) and stirred for 2 h in an ice bath (0–5 °C). Then, 6 g of $KMnO_4$ were slowly added to the resulting solution. The ice bath was removed, and the solution was then stirred at 35 °C for 2 days. An amount of 300 mL of deionized water (DI) was added gently to the solution. Then, 10 mL of H_2O_2 were slowly added to the above solution. The resulting solution was washed with HCl (400 mL, 10 %). Additional washing with DI water in order to remove the remaining contaminants and increase the pH to reach 5-6. Subsequently, the resultant aqueous concentrated GO solution was dried using a freeze dryer to produce the used GO powder.

2.3. Preparation of 3D GAM

Aqueous suspensions of GO (2.0 g L^{-1}) were prepared by adding 10 mg of GO dispersed in 5 mL deionized water via ultrasonic treatment for 20 min and the pH was adjusted to 10 by using a NH_3 solution (0.1 M). Then, 10 mg of L-ascorbic acid (vitamin C) were dissolved in a GO suspension, and the mixed suspension was transferred to a 15 mL of vial, heated to 95 °C and kept 3 h at this temperature, leading to the formation of hydrogel. Then, to remove the residual agents, the hydrogel was washed with deionized water during 24 h. Finally, the prepared graphene hydrogel was by freeze-dried for 24 h.

2.4. ALD deposition of alumina on GAM

The Al_2O_3 deposition took place in an ALD PICOSUN™ Advanced Reactor using trimethylaluminum (TMA) and water vapor as precursors. Both precursors were transferred into the chamber by separated gas lines. Nitrogen was employed as carrier gas for the precursors and purge gas. The pressure in the reaction chamber was fixed to 10 hPa and the substrate temperature to 200 °C. A deposition cycle consisted of 1 s of TMA, 30 s of purge, 1 s of water and 40 s of purge. The TMA and water exposition times were chosen considerably longer than those for typical ALD Al_2O_3 processes on flat surfaces to guarantee the precursor penetration into the GO pores. The number of deposition cycles was varied from 50 to 300 depending on the desired Al_2O_3 thickness. A growth per cycle (GPC) of 0.25 ± 0.05 nm/cycle was measured by X-ray reflectometry on a reference flat Si substrate.

The prepared hybrids are referred to as 3D Al_2O_3 / GAM-50 and 3D Al_2O_3 / GAM-300 depending on the number of ALD cycles used 50 or 300 cycles, respectively.

2.5. Material Characterization

In this study, several characterization techniques were used to investigate the samples.

Scanning electron microscopy (SEM) was carried out with a ZEISS Gemini SEM 500 equipped with a field emission gun operating at 10 kV. This SEM apparatus is also equipped with an X-ray energy dispersive spectrometer (EDS) to determine the quantitative materials composition. For SEM/EDS analyses, the samples were not previously covered by any conductive carbon or gold layer.

A Kratos Axis Ultra spectrometer equipped with a monochromatic Al Kα source (1486.6 eV) was employed for XPS analysis. For all samples, spectra were recorded at a 90° takeoff angle, with the analyzed area being currently about 0.7 × 0.3 mm². Survey spectra were acquired with 1.0 eV step and 160 eV analyzer pass energy and the high-resolution regions with 0.1 eV step and 20 eV pass energy (resolution better than 0.5 eV).

Micro-Raman spectroscopy was carried out with a Jobin Yvon LabRAM HR apparatus equipped with a CCD detector cooled to -70 °C. A 633 nm laser wavelength was used as the incident beam focused on the sample with a microscope through a wide length x100 objective and a numerical aperture of 0.50. For each sample, at least 5 spectra were recorded from different spots on the sample. For each spectrum, a background was subtracted and the maximum intensity of the D and the G bands were used to calculate the D intensity over the G intensity ratio (I_D/I_G). For each sample, one spectra with the closest values to the average I_D/I_G was chosen to be displayed.

For transmission electron microscopy (TEM) observations, a JEOL – ARM 200 F Cold FEG TEM operating at 200 kV and equipped with a spherical aberration (Cs) probe corrector was used. EDS maps were recorded on a Jeol spectrometer (SDD, Jeol DRY SD 30 GV) coupled to the transmission electron microscope. Electron energy loss spectroscopy (EELS) experiments were performed in scanning transmission electron microscopy (STEM) mode and the EEL spectrometer (Gatan GIF Quantum 965 ER) was set to an energy dispersion of 1eV/channel to

collect C-K, O-K and Al-K edges. The cross-sections were prepared by using a focused ion beam (FIB) SEM dual beam system FEI Helios NanoLab 600i.

Nitrogen adsorption isotherms were used to determine the amount of gas adsorbed at different relative pressures and the specific surface area of three samples. The surface area and pore size were evaluated by Brunauer–Emmett–Teller (BET) (Micromeritics Ltd, Dunstable, UK) standard via nitrogen adsorption at 77 K using a Micromeritics ASAP 2020 V4 volumetric adsorption apparatus and Barrett–Johner–Halenda (BJH) method, respectively, using an Autosorb 1C Quantachrome analyzer. The Langmuir adsorption isotherm model was used to fit the experimental data. The BET surface area is also known as specific surface area (SSA).

The surface charge of a sample can be calculated using its pH at zero-point charge (pH_{pzc}). Basically, zero-point charge refers to the pH at which the zeta potential is zero. A Malvern Zetasizer Nano-Z (ZEN 3600, UK) was used to determine the Zeta potential of the prepared samples in this study. Before analysis, 20 mL of deionized water were adjusted to various pH levels using 0.1 M HCl and 0.1 M NaOH solutions. Typically 20 mg of the prepared sample were added to the solution and then sonicated for 10 min. Following three measurements, the average Zeta potential was obtained.

2.6. Congo red removal study

Adsorption of Congo red (CR) on the prepared pristine 3D GAM and 3D Al_2O_3 / GAM-50 (50 ALD cycles) samples was performed by batch equilibrium tests. For the two-step adsorption process, the adsorbent (50 mg) is first immersed in the CR solution (10 mg L^{-1}, 100 mL) at pH 5 until equilibrium and next it is immersed in deionized water (pH 6.5) before being reintroduced in the pre-treated CR solution for the second step of adsorption. 2 mL of the dye solution were taken at regular intervals at every 15 min during the 60 first min of adsorption experiment and

every 120 min after this first hour and analyzed using a UV–visible spectrophotometer (Model Shimadzu UV- 1800, Japan). The concentration of the treated sample was measured at a wavelength of 663 nm. The removal of CR ξ (%) was calculated using equation (1) :

$$\zeta = \frac{C_0 - C_t}{C_0} \times 100 \qquad \text{Eq. (1)}$$

Where C_0 (mg L^{-1}) is the initial CR concentration and C_t (mg L^{-1}) is the CR concentration at a given time.

3. Results and discussion

3.1. 3D porous all-rGO monoliths

The studied 3D Al_2O_3/GAM hybrids were synthesized by a two-step approach by first self-assembling GO to form porous 3D GAMs and then depositing Al_2O_3 coating by ALD (Fig. 1). The used modified Hummers' method successfully produced thin GO nanosheets of several layers only as expected for GO material (Fig. 1a and Fig. S1, Supporting Information). GO nanosheets were well dispersed in water thanks to repulsive electrostatic forces originating from ionization of the surface functional groups such as carboxyl groups at the used high pH range (around 10) (Fig. S2, Supporting Information) [31]. The self-assembly phenomenon was induced by addition of vitamin C. The chemical reduction underwent by GO surface groups are responsible to kill the repulsive forces and lead a spontaneous assembly of the formed rGO into 3D porous GAMs [32]. In the GO solution at 2 mg mL^{-1}, the nanosheets were oriented randomly while retaining their disorder in the formed aerogels (Fig. 1b). The shape and size of the prepared GAM piece depend on the size of the recipient used for the self-assembly process. In this study, the prepared GAM have a cylinder shape of around 1 cm in diameter and 1 cm in height (Fig. 1). After freeze-drying, Al_2O_3 was deposited on the GAM surface by ALD (Fig. 1c).

Figure 1 Scheme of 3D Al_2O_3 / GAM synthesis: a) production of GO by the modified Hummers' method; b) self-assembly of GO into porous GAM; c) alumina deposition on 3D GAM surface by ALD.

SEM observations of the produced 3D GAMs show voids of a wide range of sizes (Fig. 2). The graphene layers appear suite thin with no obvious sign of stacking or overlapping of the nanosheets.

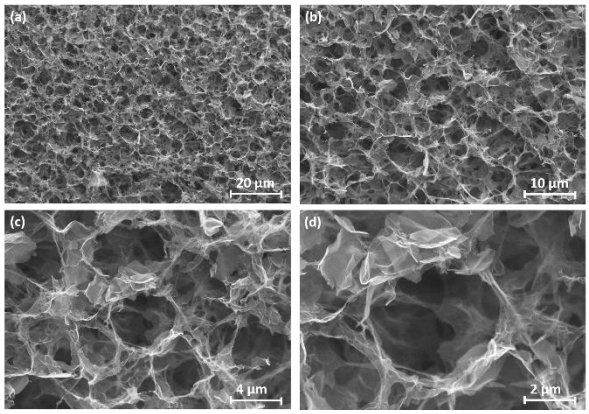

Figure 2 Representative SEM micrographs of GAMs prepared with aqueous GO dispersion; from (a) to (d), from low to high magnifications.

GO and GAM has been investigated by XPS. The atomic O/C ratios are 0.028 and 0.07 for GO and GAM, respectively; showing a significant reduction in oxygen content after the self-assembly process. Figure 3 shows XPS spectra of the starting GO and GAM samples. The deconvoluted high resolution C1s region spectra of GO and GAM are presented in Figures 3a and 3b. The contributions in the 285.0–285.7 eV region are assigned to the sp^2/sp^3 carbon atoms in C=C graphene network and/or carbon atoms belonging to C-H bonds. Higher C1s binding energy can be assigned to carbon linked to oxygen: C-O around 287 eV, C=O around 288.5 eV, and O=C-O around 289 eV [33]. As commonly observed for GO, the contributions related to carbon linked to oxygen are strongly pronounced because the high number of oxygen-containing groups GO bears (Fig. 3a). The XPS C1s signature of GAM is typical to that of reduced GO (rGO) showing a reduction in intensity of the C-O / C=O bond contributions (Fig. 3b) which evidences the reduction reaction by vitamin C when GO is self-assembled in GAM, as expected.

C1s feature of GAM shows that this reduction reaction is only partial and that oxygen-containing functional groups, which will serve as anchoring sites of the subsequent alumina deposit by ALD, are remaining at the 3D GAM surface.

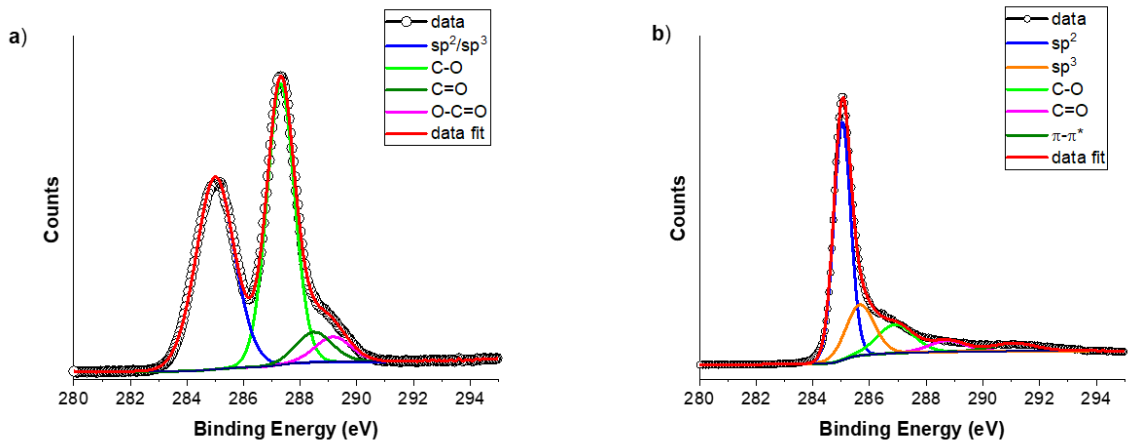

Figure 3 C1s XPS spectra of (a) the starting GO and (b) GAM samples.

3.2. 3D porous monoliths of alumina / GAM hybrids

In this study, alumina films have been deposited with two different thicknesses by varying the number of ALD cycles (50 and 300 cycles) under the same deposition temperature (200°C) and pulse/purge conditions. In this work, TMA and H_2O vapor pulse duration (1 s TMA / 30 s of purge /1 s water vapor / 40 s of purge) have been in particular chosen much longer than the standard purge conditions (0.1 s TMA pulse / 4 s water vapor pulse / 6 s purge) [34] in order to facilitate the diffusion of precursor molecules into the porous structure. By doing so, penetration is expected to be deeper into the material, which is particularly crucial for obtaining an homogeneous coating within the entire porous GAM. By using the above mentioned conditions for alumina deposition by ALD, the GPC around 0.25 nm/cycle on Si substrate (Fig. S3, Supporting Information) is found to be higher than that usually reported for ALD alumina deposition, which is due to the relatively long pulse and purge sequence used in this work [35].

Al_2O_3 nature of the deposit was evidenced by XPS analysis (Fig. S4, Supporting Information). The binding energy for Al2p can be decomposed with one contribution at 76.2 eV in good agreement with Al^{3+} [36]. The oxygen signal mainly shows two components respectively at 532.6 and 534.1 eV which can be assigned to O^{2-} and C-O-C, respectively [33,36].

For the thinnest film, SEM observations on the cross section of the 3D Al_2O_3 / GAM hybrids show a homogeneous dispersion of particles on the rGO surface (Figs. 4a and 4b). Even if the analyzed volume by EDS does not only include the extreme surface of the 3D Al_2O_3 / GAM, these particles seem to form protrusions on the top of a thin continuous film since aluminum is homogeneously detected on the whole analyzed sample area (Fig. S5, Supporting Information). When the number of ALD cycles is increased, the good covering of the GAM surface is obvious on SEM images under the form of a bulging film which significantly enlarges the GAM wall thickness (Figs. 4c and 4d).

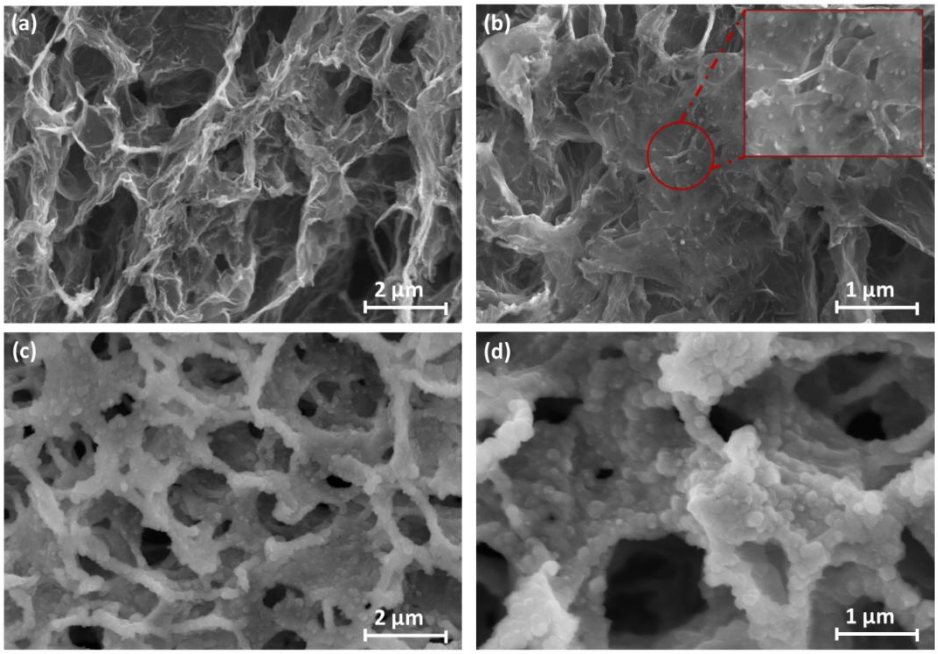

Figure 4 Typical SEM micrographs of 3D Al_2O_3/GAM hybrids prepared using two different number of ALD cycles; a) and b) 50 ALD cycles and c) and d) 300 ALD cycles.

Raman spectroscopy is a commonly used technique to investigate structural property modification of carbon nanomaterials including graphene from the intensity of the D band (around 1330 cm^{-1}) which is expected to increase in the case of introduction of defects or functional groups of the sp^2-hybridized carbon atoms. The G band (around 1590 cm^{-1}) comes from the vibrations of the C=C bonds of the sp^2 network. Raman spectra of GAM before and after ALD (300 cycles) are shown in Figure 5.

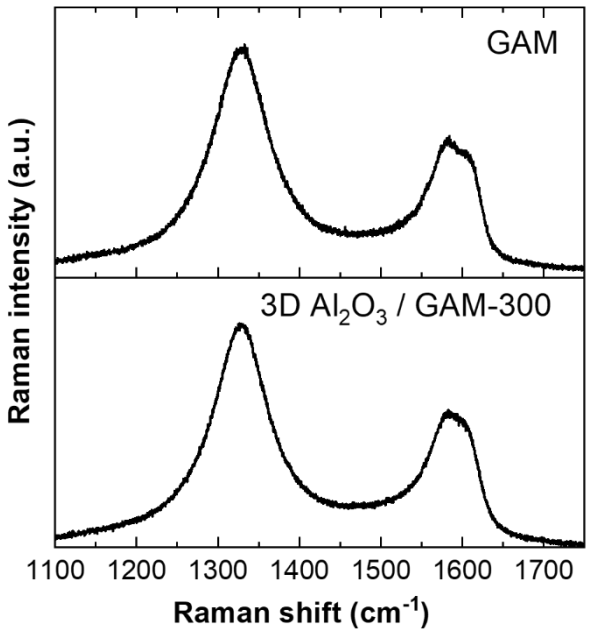

Figure 5 Raman spectroscopy spectra of the 3D GAM before and after 300 cycles of Al_2O_3 deposit by ALD (3D Al_2O_3 / GAM-300).

The Raman spectra of the GAM samples before and after alumina deposition are quite similar (Fig. 5). The calculated I_D/I_G is of 1.8 ± 0.1 and 1.8 ± 0.2, for GAM and 3D Al_2O_3 / GAM-300, respectively. The commonly used temperature for alumina deposition with TMA and water is 300°C. For this work, temperature was intentionally lessen down to 200°C with a double objective: i) to avoid elimination of the oxygen remaining functional groups remaining on GAM serving as anchoring sites for alumina growth and ii) to avoid damaging (or even consumption) of the GAM substrate during the ALD process.

The structural and chemical analyses of the inner part of the prepared 3D Al_2O_3 / GAM hybrids has been investigated by means of TEM/STEM performed on a thin lamella of around 10

micron-deep prepared by FIB (Fig. 6). The porosity and interconnected network evidenced by SEM (Fig. 4) are also evidenced in Fig. 6a. Moreover, these results provide a tangible demonstration of the technical feasibility to prepare FIB lamellas of such highly porous samples, which has been seldom reported in the literature. EDS mapping was performed to check the deposition of aluminum and oxygen within the internal pores of the 3D GAMs. Aluminum and oxygen, with similar position in the EDS maps, are detected on the graphene surface with a good coverage (Figs. 6b-6d).

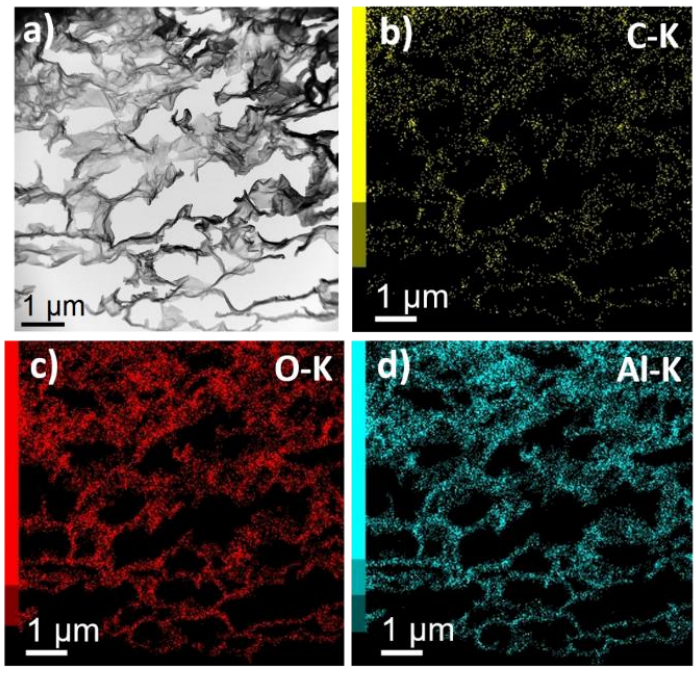

Figure 6 a) STEM bright field micrograph of the 3D alumina / GAM-300; EDS maps of b) carbon, c) aluminum and d) oxygen, respectively.

High resolution TEM/STEM observations and EELS mapping performed at some internal areas of the FIB lamella taken from 3D Al_2O_3 / GAM hybrid-300 (Fig. 7 and Fig. S6, Supporting Information) reveal the rGO layers sandwiched in between two layers of Al_2O_3 which covers both sides of nanosheets in a conformal manner.

The electron microscopy study of the prepared 3D ALD Al_2O_3 / GAM hybrids has shown that the gaseous precursors are able to diffuse within the 3D rGO network and that alumina seeding on the rGO surface is efficient enough to make grow a layer of alumina at the whole surface of the porous material, including at the internal rGO walls.

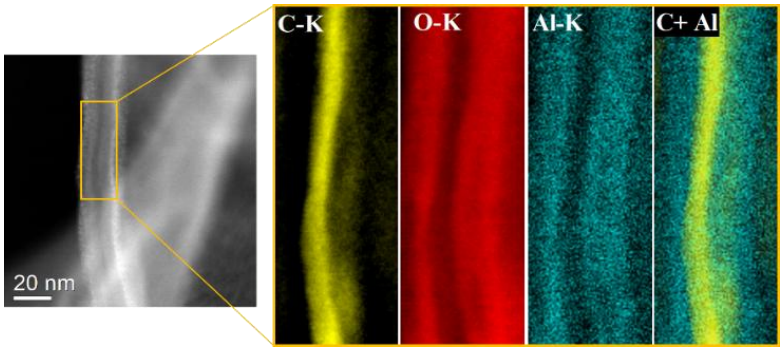

Figure 7 High resolution STEM dark field image of a folding edge evidencing the Al_2O_3 film deposited on both surfaces of 3D Al_2O_3 / GAM-300 hybrid and EELS mapping of the zone highlighted by the orange rectangle.

3.3. Mechanism of alumina deposit by ALD

For the alumina deposited with 300 ALD cycles, the thickness of the alumina layer on GAM is estimated to be approx. 7 – 8 nm (from HRTEM and EELS mapping, Fig. 7 and Fig. S6, Supporting Information) while that of alumina deposited during the same ALD run on a silicon

substrate was measured at approx. 60 nm. Inherently, the deposition process by ALD strongly depends on the nature of the substrate and especially of the number of available sites for the ALD precursor chemisorption [37]. Although in defect-free or low defect density graphene surfaces, ALD nucleation is unfavorable [24,25,38], here, the remaining functional groups on rGO (evidenced by XPS) and other present defects certainly provides favorable reactive sites for chemisorption of the precursor molecules at the early stages of the nucleation process. The growth mechanism on the rGO surface is indeed certainly initiated by a direct reaction between TMA and reactive sites at GAM surface groups like –OH and C=O. The adsorption of $Al(CH_3)_3$ with hydroxyl-OH groups initiates the first half-reaction. When $Al(CH_3)_2$ is adsorbed onto all available OH groups by a spontaneous coordination between Al and O, an Al-O bond is formed. In the second half-reaction, H_2O molecules react with the surface intermediates of $Al(CH_3)_2$ to produce CH_4 species as a product (Fig. S7, Supporting Information). TMA and H_2O molecules are thus trapped in the subsurface and form nucleation clusters. At the subsequent cycles, the space in between the alumina protrusions is filled and eventually closed to form a film of a certain roughness [39]. This statement is highly supported by the evidence shown in the SEM images in Fig. 4 confirming the preservation of the interconnected 3D rGO network architecture.

The surface area and porosity of the prepared 3D GAMs including both pristine and hybrids were determined using nitrogen adsorption isotherms. Surface area, volume and pore size are gathered in Table 1 (additional data are shown in Fig. S8, Supporting Information). The developed pristine 3D GAM shows a BET surface area of 331 m^2 g^{-1}. For 3D Al_2O_3 /GAM hybrids-50, the surface area is slightly reduced to 284 m^2/g. This surface area value is relatively high compared to other works using the same self-assembly approach [15]. When the thickness of Al_2O_3 increases (ALD cycle number increased), the surface area decreases due to the presence

of the covering layer: 284 and 32 m^2 g^{-1} for 3D Al_2O_3 / GAM-50 and 3D Al_2O_3 / GAM hybrid-300, respectively. The thicker alumina layer (deposited with 300 ALD cycles) induces a significant reduction of the BET surface of the 3D Al_2O_3 / GAM while the reduction in surface is much lower for the hybrid prepared after an ALD deposition condition of 50 cycles. After ALD deposition, the pore volume is highly diminished for 3D Al_2O_3 / GAM-300 (0.07 cm^3 g^{-1}) compared to 3D Al_2O_3 / GAM-50 (0.37 cm^3 g^{-1}) and with respect to 3D GAM (0.80 cm^3 g^{-1}).

The porous structure seems complicated with a wide range of void sizes which makes difficult their evaluation. The pore size distribution exhibits variations in the pore size distribution between samples before and after ALD deposition (Fig. S8, Supporting Information). The pore distribution of pristine 3D GAM shows two peaks at around 18 and 35 nm, which corresponds to mesoporous structures, while after deposition of 50 and 300 ALD cycle to deposit alumina, the size of the pores enlarge up to 120 nm. This could be attributed to the existence of the coating, which may cause small pores to be entirely filled or partially blocked, resulting in the absence of specific-sized micropores and mesopores within the stacked structure. In agreement with the work by George *et al*. who found that all ALD overcoated supports lost surface area due to filling of pores and interstitial voids [40]. In Table 1, the pore sizes given correspond to the average values evaluated by BET model. The N_2 adsorption versus desorption isotherm indicated that the deviation for 3D GAM is small and sharp. In principle, all the samples were purged with N_2 gas at 450°C to remove moisture and other volatile species. Once the samples were exposed to a low pressure of adsorptive gas (Fig. S8a, point A), N_2 adsorption occurred at the surface of the pristine 3D GAM, forming a monolayer (Fig. S8a, point B). As the sorption process moves through multiple layers, more N_2 molecules are adsorbed and smaller pores typically fill before larger pores (Fig. S8a, point C). A further increase in gas pressure leads to the formation of

capillary condensation (Fig. S8a, point D) which completes the adsorption branch of the isotherm. Following the pore size measurements, the pressure is reduced, and during the desorption process, the diffusion of nitrogen from internal volumes is inhibited, causing a drop in the N_2 isotherm, as shown in Fig. S8a (points E and F) at a P/P_0 of approximately 0.20. The IUPAC classification assigns the hysteresis loop of all the samples to the H3 type, which corresponds to the hypothetical slit-like porosity that can be expected in systems. Similarly, the deviations in the N_2 adsorption–desorption isotherms for 3D Al_2O_3 / GAM-50 and 3D Al_2O_3 / GAM-300 appear to be small and steep desorption branch was observed in both samples, approaching the relative pressure of 0.80. This result can either be attributed to pore-blocking over a small range of pores or to cavitation-induced evaporation [41].

Table 1 Surface area, pore volume, and pore size of pristine 3D GAM, 3D Al_2O_3 / GAM-50 and Al_2O_3 / GAM-300 hybrids.

Sample name	Surface area (m^2/g)	Pore volume (cm^3/g)	Pore size (nm)
3D GAM	331	0.80	9.88
3D Al_2O_3 / GAM-50	284	0.37	5.04
3D Al_2O_3 / GAM-300	32	0.07	7.64

George *et al.* found that all ALD overcoated supports lost surface area due to filling of pores and/or interstitial voids within the porous material [42]. The pore size remains in the same range (5 to 10 nm) before and after alumina deposition. Since the mean pore size is in the nanometer

range, the deposition of alumina on the rGO surface induces a progressive decrease of the pore size and the smallest pores are filled. Such a phenomena explains the reduction of the measured surface and pore volume. On the other hand, the available alumina surface due to the additional roughness is increased. If the alumina layer is too thick (ALD-300 cycles), the surface increase due to the created roughness does not balance the lost in surface due to the filling of the porosity. The surface of the 3D Al_2O_3 / GAM-50 hybrid developed in this study has been compared to other prepared porous alumina developed for environmental applications (Table 2). Among the reported works on alumina-based adsorbents for pollutant adsorption, only our work use the ALD approach for alumina deposition and the surface of our 3D Al_2O_3 / GAM-50 hybrid falls in the high range of the reported surface areas. Most of the prepared alumina based adsorbent have been rested for CO_2 capture or adsorption of ammonia. Al-Saliki *et al.* [43] and Renuka *et al.* [44] have studied porous and mesoporous alumina-based adsorbents for CR removal. Al Salihi *et al.* synthesized highly porous γ-Al_2O_3 nanoshells from alumina coated on carbon black (CB) by a method called Condense Layer Deposition (CLD) [45]. They studied CR adsorption (initial concentration range: 20-160 mg L^{-1} at pH range: 4-10) for their porous γ-Al_2O_3 nanoshells and they found that equilibrium for CR adsorption was reached in 30 min, much longer than that found for our alumina / GAM hybrid (Fig. 8). They did not perform any cycling study and they obtained a removal adsorption capacity for porous γ-Al_2O_3 nanoshells of 98.6 % at pH 4 which is comparable with our study. In the work by Renuka *et al.* [44], mesoporous alumina was synthesized by using the commonly used approach consisting of an aluminum precursor (aluminium isopropoxide) in the presence of dodecylamine via post hydrolysis route. Their porous alumina exhibiting a worm-like interconnected network with average pore diameter in the 3–12 nm range allowing to an efficient CR adsorption, however, the adsorption equilibrium was

reached only after around 350 min. Contrary to our adsorbent which is a non-fragmented monolith, the already reported adsorbents were under the form of nanopowders which reduces the ability for handling and recycling.

Table 2 Surface area of porous alumina-based materials and their respective targeted application from literature.

Sample Name	**Surface area (m^2 g^{-1})**	**Synthesis Method**	**Application**	**Ref.**
3D Al_2O_3 / GAM-50	284	alumina deposited by ALD	removal of CR	This work
Hybrid layered double hydroxides/mesoporous alumina (LDH/MA)	278	Surfactant-assisted self-assembly method + Co-precipitation method	CO_2 capture	[46]
Ordered mesoporous alumina	305	Evaporation-induced self-assembly	CO_2 capture and dye separation	[47]
Bead-shaped mesoporous alumina	267	Template-assisted sol–gel reaction of alumina with chitosan	Adsorption of ammonia	[48]

		as a template.		
Mesoporous alumina	95 - 289	Evaporation Induced Self Assembly (EISA) method.	Adsorption of ammonia	[49]
Porous γ-alumina nanoshells	218	Condensed layer deposition (CLD) technique	Removal of CR	[45]
Mesoporous γ-alumina	123	Post hydrolysis route adopting neutral surfactant	Removal of CR	[44]

3.4. Congo red adsorption performances

For dye removal, pH in the polluted medium is an important factor which can dramatically impact the adsorption process because it affects the surface charge of both the adsorbent and the adsorbate. In an aqueous solution, electrostatic interactions between charged surface and ionized species in the surrounding medium can be considered as powerful attractive forces. This is the reason why, Zeta Potential analysis was first investigated to determine the point of zero charge (pH_{PZC}) for the charge characteristics of the adsorbent (Fig. S9). The point of zero charge, pH_{PZC}, of 3D Al_2O_3 / GAM-50 is around 6.0 with a surface positively charged at $pH < pH_{PZC}$, and negatively charged at $pH > pH_{PZC}$.

Pristine 3D GAM and 3D Al_2O_3 / GAM-50 hybrid adsorbents have been tested for the removal of CR at pH 5 through a two-step process aiming at mimicking the use of such pollutant adsorbent in further real conditions. The adsorbent (pristine or hybrid) was first immersed in a CR solution at pH 5 and the adsorbed CR was afterwards desorbed in deionized water (pH 6.5) before performing a second adsorption test in the already pre-purified CR solution. For the first step of CR removal (Fig. 8a), the adsorption of CR on 3D Al_2O_3 / GBM-50 hybrid is faster than that observed for 3D pristine GAM and reaches equilibrium after only 15 min with a CR removal yield of 87 % while CR is adsorbed less rapidly and less efficiently on 3D pristine GAM (20 % of CR removed after 30 min). At the second adsorption step, 98 % of CR removal are calculated for the porous alumina adsorbent while for pristine 3D GAM no adsorption occurs at the second adsorption step.

CR is an anionic standard dye at its natural pH (pH 5) [50] at which the CR adsorption performance was studied. At the used pH<, pH_{PZC}, during the adsorption process, Al_2O_3 / GAM-50 positively charged promoted an efficient adsorption of the negatively charged CR dye. CR was subsequently easily desorbed from the alumina surface since the desorption process occurred in deionized water (pH around 6.5), the used hybrid adsorbent falling in its neutral-negative charge zone. At the second cycle, the adsorption sites were available again to adsorb the remaining CR molecules reaching that way an adsorption yield of 98 %.

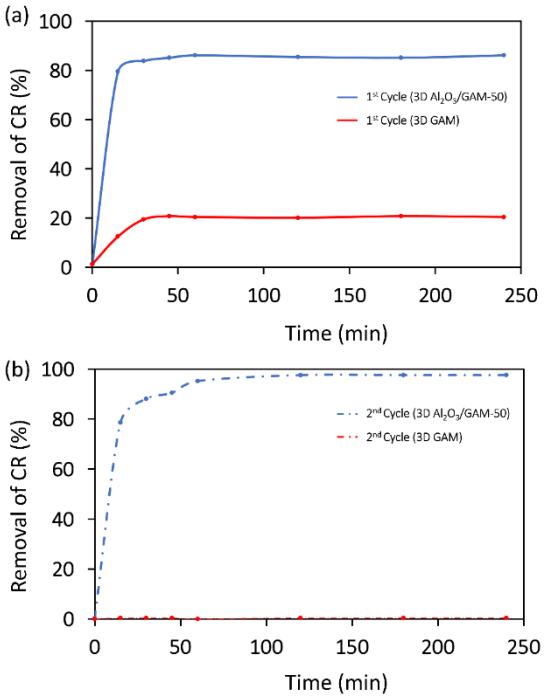

Figure 8 Adsorption isotherms for pristine 3D GAM and 3D Al_2O_3/GAM-50 hybrid (a) first step and (b) second step.

Conclusion

Alumina has been successfully deposited on rGO nanosheets within a macroscopic porous graphene (GAM). Contrary to standard metal-based particles or film deposit methods (impregnation, CVD), ALD approach has been proved to provide a facile access to the internal porosity of the complex morphology of macroscopic porous rGO leading to exploit the whole available surface offered by the rGO walls of GAMs. The growth mechanism of alumina on the rGO surface of GAMs involves a nucleation process forming first islands and finally a well covering layer. From the proposed mechanism, the developed assembly process indeed provides

the required seeding sites on rGO for its full coverage which is rarely observed in literature without using additives such as polymers, or surfactants. The developed ALD 3D Al_2O_3 / GAM hybrid has been tested for CR removal. The results have shown a higher adsorption capacity than that measured for pristine 3D GAM thanks to favorable interactions between alumina surface and CR in the used conditions. Moreover, mass transfer of CR dye molecules between liquid solution and alumina surface is as well certainly not a limiting factor due to the multi-porosity offered by the hybrid guaranteeing an ease of access to the adsorption sites. Another impacting result relates with the successful investigation of technically advanced approaches for an in-depth characterization of 3D porous alumina / GAM hybrids which are nanomaterials difficult to analyze especially because of the complexity of their three-dimensional structure.

Supporting information

The following file is available free of charge: TEM images of GO, EDS analysis of the hybrids, TEM/HRTEM of the hybrids, ALD mechanism, isotherms from adsorption volumetry, Zeta potential.

Author Contributions

Experiments, methodology, graphene oxide synthesis, adsorption measurements, writing and data analysis: R.M.F.; ALD deposit, data analyzing, review and editing: C.M.; FIB lamella preparation: S.M.; TEM imaging and analysis: M.E.; data analyzing, methodology, writing, review and editing: JFP; supervision, project administration and funding acquisition: A.R.M.; supervision project administration, data analyzing and fitting, methodology, writing, review and editing: B.V.

Acknowledgments

The authors would like to thank the technical platforms “Microscopies, Microprobes and Metallography (3M)”, “Synthesis and Analysis of Nanomaterials in Ultra-high vacuum (CC D.A.U.M.)” and “Optic and Lasers Competence Center (CC OL)” at Institut Jean Lamour (IJL, Nancy, France) for access to TEM, SEM, ALD and Raman spectroscopy equipment facilities, respectively. B.V. thanks the platform “Spectroscopies et Microscopies des Interfaces” (Laboratory of Physical Chemistry and Microbiology for Materials and the Environment, LCPME, Nancy, France) and A. Renard, Dr. M. Mallet (LCPME) for XPS analysis. The authors thank Alexandre Bouché for his valuable help for ALD deposit.

Conflicts of interest

The authors are no conflicts to declare.

References

[1] H. Wang, H. Dai, Strongly coupled inorganic–nano-carbon hybrid materials for energy storage, Chem. Soc. Rev. 42 (2013) 3088–3113. https://doi.org/10.1039/C2CS35307E.
[2] Q. Hu, G. Li, Z. Han, Z. Wang, X. Huang, H. Yang, Q. Zhang, J. Liu, C. He, Recent progress in the hybrids of transition metals/carbon for electrochemical water splitting, J. Mater. Chem. A. 7 (2019) 14380–14390. https://doi.org/10.1039/c9ta04163j.
[3] H. Wang, Q. Chen, S. Zhou, Carbon-based hybrid nanogels: a synergistic nanoplatform for combined biosensing, bioimaging, and responsive drug delivery, Chem. Soc. Rev. 47 (2018) 4198–4232. https://doi.org/10.1039/c7cs00399d.
[4] M.K.M. Azim, A. Arifutzzaman, R. Saidur, M.U. Khandaker, D.A. Bradley, Recent progress in emerging hybrid nanomaterials towards the energy storage and heat transfer applications: A review, J. Mol. Liq. 360 (2022) 119443. https://doi.org/10.1016/j.molliq.2022.119443.
[5] A.G. Navrotskaya, D.D. Aleksandrova, E.F. Krivoshapkina, M. Sillanpää, P.V. Krivoshapkin, Hybrid Materials Based on Carbon Nanotubes and Nanofibers for Environmental Applications, Frontiers in Chemistry. 8 (2020). https://www.frontiersin.org/articles/10.3389/fchem.2020.00546 (accessed November 11, 2022).

[6] B. Xia, Y. Yan, X. Wang, X.W. (David) Lou, Recent progress on graphene-based hybrid electrocatalysts, Mater. Horiz. 1 (2014) 379–399. https://doi.org/10.1039/C4MH00040D.
[7] The murky future of global water quality: New global study projects rapid deterioration in water quality, (n.d.). https://ebrary.ifpri.org/digital/collection/p15738coll2/id/129349 (accessed November 9, 2022).
[8] E.P. Fernandes, T.S. Silva, C.M. Carvalho, R. Selvasembian, N. Chaukura, L.M.T.M. Oliveira, S.M.P. Meneghetti, L. Meili, Efficient adsorption of dyes by γ-alumina synthesized from aluminum wastes: Kinetics, isotherms, thermodynamics and toxicity assessment, Journal of Environmental Chemical Engineering. 9 (2021) 106198. https://doi.org/10.1016/j.jece.2021.106198.
[9] R. Azhdari, S.M. Mousavi, S.A. Hashemi, S. Bahrani, S. Ramakrishna, Decorated graphene with aluminum fumarate metal organic framework as a superior non-toxic agent for efficient removal of Congo Red dye from wastewater, Journal of Environmental Chemical Engineering. 7 (2019) 103437. https://doi.org/10.1016/j.jece.2019.103437.
[10] D.K. Jambhulkar, R.P. Ugwekar, B.A. Bhanvase, D.P. Barai, A review on solid base heterogeneous catalysts: preparation, characterization and applications, Chemical Engineering Communications. 209 (2022) 433–484. https://doi.org/10.1080/00986445.2020.1864623.
[11] P.O. Oviroh, R. Akbarzadeh, D. Pan, R.A.M. Coetzee, T.-C. Jen, New development of atomic layer deposition: processes, methods and applications, Science and Technology of Advanced Materials. 20 (2019) 465–496. https://doi.org/10.1080/14686996.2019.1599694.
[12] P. Munnik, P.E. de Jongh, K.P. de Jong, Recent Developments in the Synthesis of Supported Catalysts, Chem. Rev. 115 (2015) 6687–6718. https://doi.org/10.1021/cr500486u.
[13] K.S. Novoselov, V.I. Fal′ko, L. Colombo, P.R. Gellert, M.G. Schwab, K. Kim, A roadmap for graphene, Nature. 490 (2012) 192–200. https://doi.org/10.1038/nature11458.
[14] N. Yousefi, X. Lu, M. Elimelech, N. Tufenkji, Environmental performance of graphene-based 3D macrostructures, Nat. Nanotechnol. 14 (2019) 107–119. https://doi.org/10.1038/s41565-018-0325-6.
[15] R.M. Firdaus, N. Berrada, A. Desforges, A.R. Mohamed, B. Vigolo, From 2D Graphene Nanosheets to 3D Graphene-based Macrostructures, Chem.-Asian J. 15 (2020) 2902–2924. https://doi.org/10.1002/asia.202000747.
[16] M. Etesami, M.T. Nguyen, T. Yonezawa, A. Tuantranont, A. Somwangthanaroj, S. Kheawhom, 3D carbon nanotubes-graphene hybrids for energy conversion and storage applications, Chemical Engineering Journal. 446 (2022) 137190. https://doi.org/10.1016/j.cej.2022.137190.
[17] H. Liu, H. Qiu, Recent advances of 3D graphene-based adsorbents for sample preparation of water pollutants: A review, Chem. Eng. J. 393 (2020) 124691. https://doi.org/10.1016/j.cej.2020.124691.
[18] H. Vijwani, M.N. Nadagouda, V. Namboodiri, S.M. Mukhopadhyay, Hierarchical hybrid carbon nano-structures as robust and reusable adsorbents: Kinetic studies with model dye compound, Chemical Engineering Journal. 268 (2015) 197–207. https://doi.org/10.1016/j.cej.2015.01.027.
[19] X. Zhang, J. Zhou, Y. Zheng, H. Wei, Z. Su, Graphene-based hybrid aerogels for energy and environmental applications, Chemical Engineering Journal. 420 (2021) 129700. https://doi.org/10.1016/j.cej.2021.129700.

[20] U. Kamran, K.Y. Rhee, S.-Y. Lee, S.-J. Park, Innovative progress in graphene derivative-based composite hybrid membranes for the removal of contaminants in wastewater: A review, Chemosphere. 306 (2022) 135590. https://doi.org/10.1016/j.chemosphere.2022.135590.
[21] X. Chen, J. Tao, Y. Liu, R. Bao, F. Li, C. Li, J. Yi, Interface interaction and synergistic strengthening behavior in pure copper matrix composites reinforced with functionalized carbon nanotube-graphene hybrids, Carbon. 146 (2019) 736–755. https://doi.org/10.1016/j.carbon.2019.02.048.
[22] M. Khan, M.N. Tahir, S.F. Adil, H.U. Khan, M.R.H. Siddiqui, A.A. Al-warthan, W. Tremel, Graphene based metal and metal oxide nanocomposites: synthesis, properties and their applications, J. Mater. Chem. A. 3 (2015) 18753–18808. https://doi.org/10.1039/C5TA02240A.
[23] H.-F. Wang, C. Tang, Q. Zhang, A review of graphene-based 3D van der Waals hybrids and their energy applications, Nano Today. 25 (2019) 27–37. https://doi.org/10.1016/j.nantod.2019.02.006.
[24] R.H.J. Vervuurt, W.M.M. (Erwin) Kessels, A.A. Bol, Atomic Layer Deposition for Graphene Device Integration, Advanced Materials Interfaces. 4 (2017) 1700232. https://doi.org/10.1002/admi.201700232.
[25] X. Wang, S.M. Tabakman, H. Dai, Atomic Layer Deposition of Metal Oxides on Pristine and Functionalized Graphene, J. Am. Chem. Soc. 130 (2008) 8152–8153. https://doi.org/10.1021/ja8023059.
[26] L. Zheng, X. Cheng, D. Cao, G. Wang, Z. Wang, D. Xu, C. Xia, L. Shen, Y. Yu, D. Shen, Improvement of Al2O3 Films on Graphene Grown by Atomic Layer Deposition with Pre-H2O Treatment, ACS Appl. Mater. Interfaces. 6 (2014) 7014–7019. https://doi.org/10.1021/am501690g.
[27] D.R. Dreyer, S. Park, C.W. Bielawski, R.S. Ruoff, The chemistry of graphene oxide, Chem. Soc. Rev. 39 (2010) 228–240. https://doi.org/10.1039/b917103g.
[28] S. Pei, H.-M. Cheng, The reduction of graphene oxide, Carbon. 50 (2012) 3210–3228. https://doi.org/10.1016/j.carbon.2011.11.010.
[29] Y. Lin, Y. Tian, H. Sun, T. Hagio, Progress in modifications of 3D graphene-based adsorbents for environmental applications, Chemosphere. 270 (2021) 129420. https://doi.org/10.1016/j.chemosphere.2020.129420.
[30] W.S. Hummers, R.E. Offeman, Preparation of Graphitic Oxide, J. Am. Chem. Soc. 80 (1958) 1339–1339. https://doi.org/10.1021/ja01539a017.
[31] B. Konkena, S. Vasudevan, Understanding Aqueous Dispersibility of Graphene Oxide and Reduced Graphene Oxide through pKa Measurements, J. Phys. Chem. Lett. 3 (2012) 867–872. https://doi.org/10.1021/jz300236w.
[32] Z. Yuan, X. Xiao, J. Li, Z. Zhao, D. Yu, Q. Li, Self-Assembled Graphene-Based Architectures and Their Applications, Advanced Science. 5 (2018) 1700626. https://doi.org/10.1002/advs.201700626.
[33] R. Al-Gaashani, A. Najjar, Y. Zakaria, S. Mansour, M.A. Atieh, XPS and structural studies of high quality graphene oxide and reduced graphene oxide prepared by different chemical oxidation methods, Ceramics International. 45 (2019) 14439–14448. https://doi.org/10.1016/j.ceramint.2019.04.165.

[34] I. Iatsunskyi, M. Kempiński, M. Jancelewicz, K. Załęski, S. Jurga, V. Smyntyna, Structural and XPS characterization of ALD Al2O3 coated porous silicon, Vacuum. 113 (2015) 52–58. https://doi.org/10.1016/j.vacuum.2014.12.015.
[35] S.-Y. Ham, Z. Jin, S. Shin, M. Kim, M. Seo, Y.-S. Min, Investigation of abnormally high growth-per-cycle in atomic layer deposition of Al2O3 using trimethylaluminum and water, Applied Surface Science. 571 (2022) 151282. https://doi.org/10.1016/j.apsusc.2021.151282.
[36] A. Nylund, I. Olefjord, Surface analysis of oxidized aluminium. 1. Hydration of Al2O3 and decomposition of Al(OH)3 in a vacuum as studied by ESCA, Surface and Interface Analysis. 21 (1994) 283–289. https://doi.org/10.1002/sia.740210504.
[37] T. Park, H. Kim, M. Leem, W. Ahn, S. Choi, J. Kim, J. Uh, K. Kwon, S.-J. Jeong, S. Park, Y. Kim, H. Kim, Atomic layer deposition of Al2O3 on MoS2, WS2, WSe2, and h-BN: surface coverage and adsorption energy, RSC Adv. 7 (2017) 884–889. https://doi.org/10.1039/C6RA24733D.
[38] C.A. Wilson, R.K. Grubbs, S.M. George, Nucleation and Growth during Al_2O_3 Atomic Layer Deposition on Polymers, Chem. Mater. 17 (2005) 5625–5634. https://doi.org/10.1021/cm050704d.
[39] E. Schilirò, R. Lo Nigro, S.E. Panasci, F.M. Gelardi, S. Agnello, R. Yakimova, F. Roccaforte, F. Giannazzo, Aluminum oxide nucleation in the early stages of atomic layer deposition on epitaxial graphene, Carbon. 169 (2020) 172–181. https://doi.org/10.1016/j.carbon.2020.07.069.
[40] C. George, P. Littlewood, P.C. Stair, Understanding Pore Formation in ALD Alumina Overcoats, ACS Appl. Mater. Interfaces. 12 (2020) 20331–20343. https://doi.org/10.1021/acsami.9b23256.
[41] M. Thommes, K. Kaneko, A.V. Neimark, J.P. Olivier, F. Rodriguez-Reinoso, J. Rouquerol, K.S.W. Sing, Physisorption of gases, with special reference to the evaluation of surface area and pore size distribution (IUPAC Technical Report), Pure and Applied Chemistry. 87 (2015) 1051–1069. https://doi.org/10.1515/pac-2014-1117.
[42] C. George, P. Littlewood, P.C. Stair, Understanding Pore Formation in ALD Alumina Overcoats, ACS Appl. Mater. Interfaces. 12 (2020) 20331–20343. https://doi.org/10.1021/acsami.9b23256.
[43] S. Al-Salihi, A.M. Jasim, M.M. Fidalgo, Y. Xing, Removal of Congo red dyes from aqueous solutions by porous gamma-alumina nanoshells, Chemosphere. 286 (2022) 131769. https://doi.org/10.1016/j.chemosphere.2021.131769.
[44] N.K. Renuka, A.V. Shijina, A.K. Praveen, Mesoporous γ-alumina nanoparticles: Synthesis, characterization and dye removal efficiency, Materials Letters. 82 (2012) 42–44. https://doi.org/10.1016/j.matlet.2012.05.043.
[45] S. Al-Salihi, A.M. Jasim, M.M. Fidalgo, Y. Xing, Removal of Congo red dyes from aqueous solutions by porous γ-alumina nanoshells, Chemosphere. 286 (2022) 131769. https://doi.org/10.1016/j.chemosphere.2021.131769.
[46] K. Wu, Q. Ye, L. Wang, F. Meng, H. Dai, Mesoporous alumina-supported layered double hydroxides for efficient CO2 capture, Journal of CO2 Utilization. 60 (2022) 101982. https://doi.org/10.1016/j.jcou.2022.101982.
[47] G.L. Seah, L. Wang, L.F. Tan, C. Tipjanrawee, W.A. Sasangka, A.K. Usadi, J.M. McConnachie, K.W. Tan, Ordered Mesoporous Alumina with Tunable Morphologies and

Pore Sizes for CO_2 Capture and Dye Separation, ACS Appl. Mater. Interfaces. 13 (2021) 36117–36129. https://doi.org/10.1021/acsami.1c06151.
[48] J. Kim, H. Lee, H.T. Vo, G. Lee, N. Kim, S. Jang, J.B. Joo, Bead-Shaped Mesoporous Alumina Adsorbents for Adsorption of Ammonia, Materials. 13 (2020) 1375. https://doi.org/10.3390/ma13061375.
[49] H.T. Vo, J. Kim, N.Y. Kim, J.-K. Lee, J.B. Joo, Effect of pore texture property of mesoporous alumina on adsorption performance of ammonia gas, Journal of Industrial and Engineering Chemistry. 91 (2020) 129–138. https://doi.org/10.1016/j.jiec.2020.07.046.
[50] K. Litefti, M.S. Freire, M. Stitou, J. González-Álvarez, Adsorption of an anionic dye (Congo red) from aqueous solutions by pine bark, Sci Rep. 9 (2019) 16530. https://doi.org/10.1038/s41598-019-53046-z.

TABLE OF CONTENTS

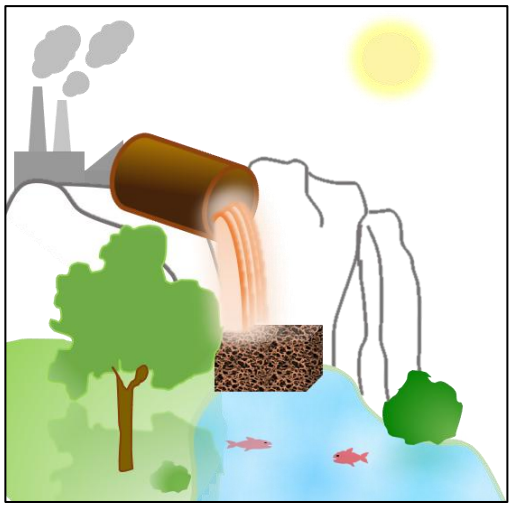

3D porous ALD alumina / reduced graphene oxide hybrid as efficient adsorbent for water treatment